Influence of boron isotope ratio on the thermal conductivity of uranium diboride (UB2) and zirconium diboride (ZrB2)

Evitts, Lee; Middleburgh, Simon; Kardoulaki, Erofili; Ipatova, Iuliia; Rushton, Michael; Lee, Bill

Journal of Nuclear Materials

DOI:
10.1016/j.jnucmat.2019.151892

Published: 01/01/2020

Peer reviewed version

Influence of boron isotope ratio on the thermal conductivity of uranium diboride (UB_2) and zirconium diboride (ZrB_2)

L.J. Evitts[a,*], S.C. Middleburgh[a], E. Kardoulaki[b], I. Ipatova[a], M.J.D. Rushton[a], W.E. Lee[a,c]

[a]*Nuclear Futures Institute, Bangor University, Bangor, Gwynedd, LL57 2DG, UK*
[b]*Los Alamos National Laboratory, Los Alamos, NM, 87545, USA*
[c]*Institute for Security Science and Technology, Imperial College London, London, SW7 2AB, UK*

Abstract

Uranium diboride is being proposed as an accident tolerant fuel (either as a part of a composite or a ^{11}B enriched monolithic fuel pellet), while zirconium diboride is often selected as a burnable absorber in conjunction with uranium dioxide fuel pellets. It is therefore important to understand the thermal properties of these materials and examine methods in which they may be improved. The thermal conductivity of UB_2 and ZrB_2 is calculated through atomic scale modelling methods. It was found that the boron-isotope ratio has a significant impact on the thermal conductivity of ZrB_2, but is negligible for UB_2 due to the large electron-phonon scattering.

Keywords: Uranium diboride, Zirconium diboride, Nuclear fuel, Thermal conductivity, Density functional theory

1. Introduction

Two of the main accident tolerant fuel (ATF) candidate materials considered for commercial use are UN and U_3Si_2, owing to their increased uranium density and thermal conductivity over UO_2 [1–4]. Compared to UO_2, both of these leading candidates for high density ATF have significantly exothermic reactions with water [5–7].

Alternative fuels such as UB_2, and fuel designs such as composites with UO_2 have subsequently been targeted [8]. ^{11}B has a slightly larger thermal neutron capture cross section than ^{16}O unlike the thermal neutron absorber ^{10}B [9] - and as such can be considered a valid fuel when isotopically enriched. The uranium density of UB_2 (11.6 g/cm^3) is comparable to that of U_3Si_2, which has a density of 11.3 g/cm^3 [1] indicating that the choice between the two fuels would be dictated by other properties. Monolithic UB_2 pellets, in addition to composite UO_2-UB_2 [10] and U_3Si_2-UB_2 pellets [11], are now being considered as an ATF. The composite fuels can take advantage of incorporating the ^{10}B isotope that will act as a burnable absorbing material - improving the fuel cycle economics of the fuel further [11, 12].

Uranium diboride (UB_2) has a hexagonal $P6/mmm$ unit cell structure [13], shown in Figure 1, and is composed of alternating layers of U and B. It is a common structure shared with many other diborides including ZrB_2, which is also used as a burnable absorber in some nuclear fuel designs [14]. Previous work has shown that UB_2 does not accommodate any significant deviations in stoichiometry and can therefore be considered a line compound in a similar manner to U_3Si_2 [15] and ZrB_2 [16].

The thermal conductivity of nuclear fuel is an important parameter that determines the behaviour of the fuel under normal operation and in the event of an anticipated operational occurrence (AOO) or accident. Not only is it important to understand fresh fuel's thermal conductivity, but also the impact that burnup has on this material property. In UO_2, the impacts of fission product concentration, radiation damage and stoichiometry have been modelled with some success [17–21]. At present, the thermal conductivity of UO_2 predicted using atomic scale methods only slightly underestimates the thermal conductivity measured experimentally. For example, Torres & Kaloni [22] calculated a lattice thermal conductivity of approximately 5.6 W/mK at 500 K, which is a little under the experimental value of 6.6 W/mK [4]. The authors assume that the contribution from electrical thermal conductivity is negligible and instead suggest that discrepancies may arise from insufficiently small super-cells or higher-order phonon processes. There has also been recent success in fitting the Callaway model to experimental data of UO_2 when the phonon-spin contribution is included [23].

The major aim of this research is to highlight the influence of the boron isotopic ratio on the thermal conductivity of UB_2 and ZrB_2 through the use of DFT calculations. The method, simulation codes and parameters used in this work are detailed in Section 2 while the results are examined in Section 3.

2. Methodology

The density functional theory (DFT) calculations in this work were performed with the Vienna Ab-initio Simulation Package (VASP) [24–27]. The projector augmented wave (PAW) potentials [28, 29] were used in conjunction with the GGA exchange

*Corresponding author
Email address: l.evitts@bangor.ac.uk (L.J. Evitts)

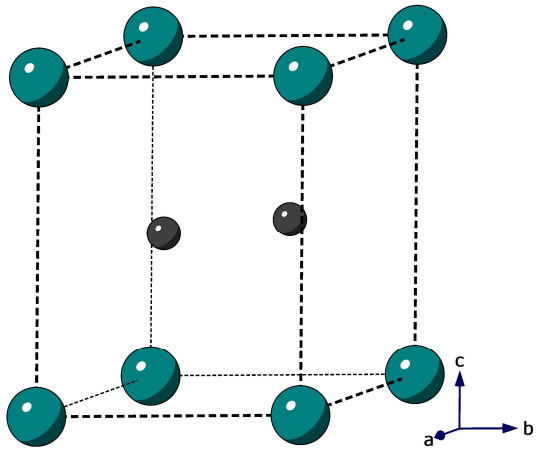

Figure 1: The hexagonal P6/mmm unit cell structure of UB_2 where the small black spheres are B atoms.

correlation functional described by Perdew, Burke and Ernzerhof [30, 31].

In all calculations a convergence threshold of 10^{-8} eV was set for electronic minimization, and a threshold of 10^{-8} eV/Å was set for geometric optimization. The cut-off energy was set to 400 eV for all calculations with a first order Methfessel-Paxton [32] smearing with a width of 0.1 eV. A Γ-centred k-point mesh was automatically generated with a constant k-point density of approximately 0.03 Å for each calculated cell size. Spin-orbit interactions were included in the calculations however, as UB_2 has previously been determined as a metallic Pauli-paramagnetic compound [33], the initial magnetization value was set at zero.

In a number of compounds it becomes necessary to introduce a term for localized d or f electrons due to the inherent electron delocalization present in DFT calculations. If this extra term, otherwise known as the Hubbard parameter, is excluded from the calculations then the band structure can be incorrectly predicted. For example, DFT calculations predict a metallic structure for UO_2 until the additional localization term is included and thereby creates a gap in the electronic band structure [34]. Authors who have previously performed DFT calculations on UB_2 have justified using either a value of 2.0 eV for the Hubbard parameter (based on lattice parameters) [35], or excluded the parameter due to an incorrect prediction for the enthalpy of formation [15]. However, it has been shown experimentally that the $5f$ electrons of UB_2 are itinerant due to the small U-U distance, which creates a large f-f overlap [36]. It is therefore not justifiable to include the localization term for DFT calculations of UB_2.

The phonon-phonon interactions, and subsequently the lattice thermal conductivity, were calculated with the Phono3py [37] package. Phono3py solves the linearized phonon Boltzmann transport equations (BTE) with a single-mode relaxation-time approximation (RTA) [37]. The approximation is made due to the high computational cost of solving the full BTE. Phono3py is also able to calculate the phonon-isotope scattering rate through second-order perturbation theory discussed in Ref [38]. Forces were calculated in VASP using a super-cell of 3×3×2 containing 54 lattice sites. The size of the super-cell was chosen based on convergence from smaller cell sizes, though larger cells were not investigated. To optimise the computational effort in repeated calculations of the lattice thermal conductivity, κ_l, a study was performed varying the cutoff pair-distance i.e. the maximum distance in which the atomic forces are calculated. It was found that convergence is achieved at a distance of 3.2 Å (i.e. the third nearest neighbour).

The BTE are separately solved using Density-Functional Perturbation Theory (DFPT) and Maximally Localized Wannier Functions (MLWF) with the electron-phonon Wannier (EPW) [39] package of Quantum ESPRESSO [40]. This allows for calculations of the electronic conductivity, electron-phonon matrix elements, and electron-phonon scattering rates. The matrix elements were first calculated with a coarse $6 \times 6 \times 6$ k-mesh and q-mesh, then interpolated with a finer $50 \times 50 \times 50$ k-mesh and q-mesh using MLWF. Spin-orbit coupling was not included in these calculations, as no acceptable norm-conserving pseudopotential was found for uranium. Separate calculations were performed using a scalar relativistic PBE and a LDA pseudopotential, which produced similar results.

3. Results & Discussion

3.1. ZrB_2

The method of calculating the lattice thermal conductivity was validated against the previous experimental results of ZrB_2, for which there is plenty of data available [41] yet is lacking for UB_2. ZrB_2 has the same crystal structure as UB_2 and similar material behaviour. The lattice thermal conductivity is obtained through DFT calculations and Phono3py using the same method and input parameters discussed in Section 2. The electronic thermal conductivity is calculated using BoltzTraP2 [42] (which can solve the BTE through smoothed Fourier interpolation of electronic bands) and the electrical resistivity measured from Ref [43].

There have been many approaches to manufacturing and measuring the thermal conductivity of ZrB_2, which are summarised in Ref [41]. The total thermal conductivity calculated in this work is compared with experiment in Figure 2. The upper and lower boundaries of the experimental data are represented by measurements from Zimmermann et al. [43] and Zhang et al. [45]. The thermal conductivity measured by Kinoshita et al. [44] was performed on a single crystal of ZrB_2 and thus best represents the results obtained through DFT calculations. It can be seen that the calculated results lie within the range of experimental data, suggesting that the method is reasonable.

The accumulated lattice thermal conductivities at 300 K, in both x and z directions, are displayed in Figure 3(a), and the associated phonon density of states in Figure 3(b). It can be seen that the acoustic low-frequency phonons from the vibrations of the Zr atoms are the dominant contributor to κ_l in the z direction. The high-frequency optical phonons, which are dominated

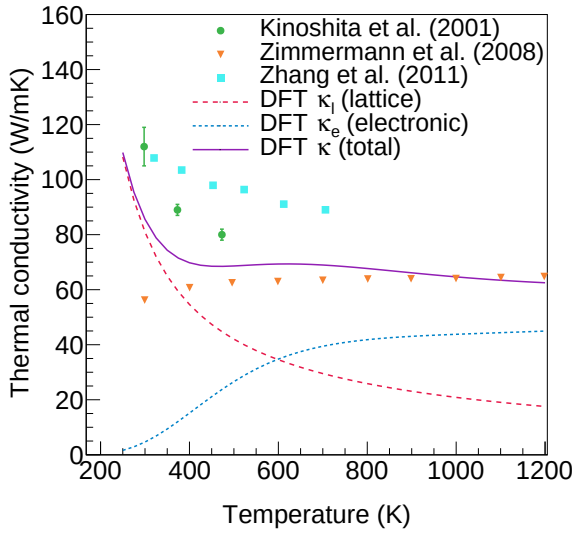

Figure 2: The calculated lattice (dashed red line), electronic (dashed blue line) and total (solid purple line) thermal conductivity of ZrB_2 compared with select experimental data [43–45].

by the vibrations of the B atoms, contribute roughly 10 % of κ_l in the x/y plane. The ratio of contributions that is displayed in Figure 3(a) is also observed at higher temperatures, not shown.

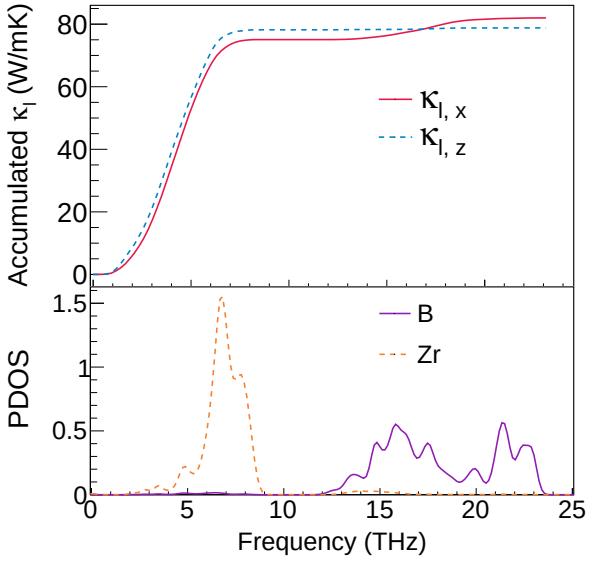

Figure 3: The calculated (a) accumulated lattice thermal conductivity at 300 K in the x and z directions, (b) the phonon density of states for ZrB_2.

The effect of the isotopic boron ratio on κ_l is easily investigated by altering the masses and mass variances with Phono3py. The difference in κ_l, relative to the natural abundance ratio of B, is shown in Figure 4. It can be seen that the greatest increase in κ_l is obtained when pure ^{11}B is used, and remains consistently high across the the studied temperature range. A similar effect is observed for pure ^{10}B but it is not as significant, and the effect decreases as temperature increases.

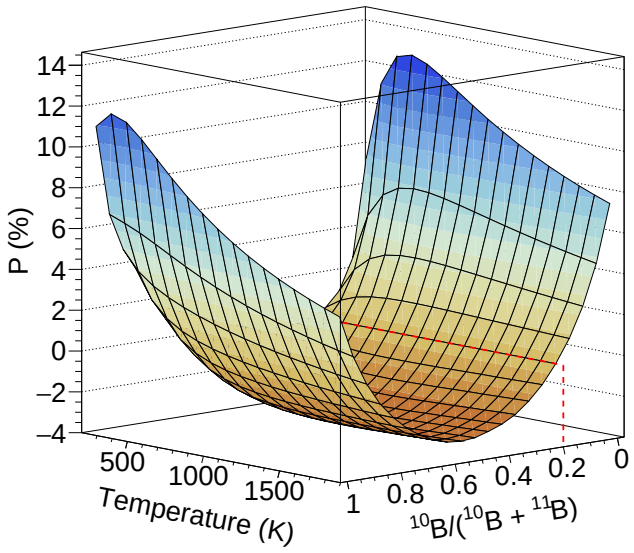

Figure 4: The percentage change, P, in the lattice thermal conductivity of ZrB_2 as a function of temperature and boron isotope ratio. P is relative to the natural abundance isotope ratio of 0.2, shown by the red dashed line. The lines of the surface are in increments of 100 K and 0.05 for the temperature and isotope ratio, respectively.

3.2. UB_2

The lattice parameters of UB_2, following the geometric relaxation of the unit cell, are calculated to be 3.084 Å and 4.020 Å for the a and c directions, respectively. This is comparable to the weighted average of previous experimental measurements, where a is 3.1302(3) Å and c is 3.9879(3) Å [13, 46–49].

The mechanical properties of UB_2 were calculated and shown in Table 1. The five elastic constants, C_{ij}, of a hexagonal crystal structure are derived from the strain-stress relationship following distortion calculations. The Hill average of the bulk modulus, B, and shear modulus, G, were calculated from the average of the Voigt and Reuss bounds, as described in Ref [50]. The Young's modulus, E, and Poisson's ratio, μ, were calculated from the bulk and shear moduli via [50]

$$\frac{1}{E} = \frac{1}{3G} + \frac{1}{9B} \tag{1}$$

$$\mu = \frac{1}{2}\left(1 - \frac{3G}{3B+G}\right) \tag{2}$$

The average sound velocity, v, was calculated from the transverse (T) and longitudinal (L) velocities of polycrystalline UB_2 via [51]

$$v_T = \sqrt{\frac{G}{D}} \tag{3}$$

$$v_L = \sqrt{\frac{B + 4/3G}{D}} \tag{4}$$

$$v^{-3} = \frac{1}{3}\left(v_L^{-3} + 2v_T^{-3}\right) \tag{5}$$

where $D = 12.7\,\mathrm{g/cm^3}$ is the density of UB_2 [52]. The Debye temperature, θ_D was calculated from [53]

$$\theta_D = \frac{\hbar v}{k_B}\left(\frac{6\pi^2 n_a}{\Omega}\right)^{1/3} \quad (6)$$

where k_B is Boltzmann's constant, n_a and Ω are the number of atoms and volume of the unit cell respectively.

Properties that have been previously calculated with DFT [35] or experimentally measured [13, 54] for UB_2 are also shown in Table 1. Compared to the DFT calculations performed by Jossou et al. [35], differences can be observed between the values of C_{ij} which produces differences in all of the subsequently derived properties. Many of the input parameters used within this work are similar to those of Jossou et al. [35] but a different code was used to obtain the results. The moduli obtained in this work agrees fairly well with the experimental measurement of Dancausse et al. [13] but differs to Kardoulaki et al. [55] where the authors suggest potential internal cracking in their sample. There is variation in the values of θ_D due to the different methods and samples e.g. Flotow et al. [54] performed their measurement at close to 0 K.

The accumulated lattice thermal conductivity at 300 K is displayed in Figure 5(a) in both x and z directions. The κ_l produced by Phono3py, which calculates phonon-phonon and phonon-isotope scattering only, was found to be 2 to 3 times larger than the experimental result [55]. The associated phonon density of states are shown in Figure 5(b), exhibiting a similar behaviour to that of ZrB_2.

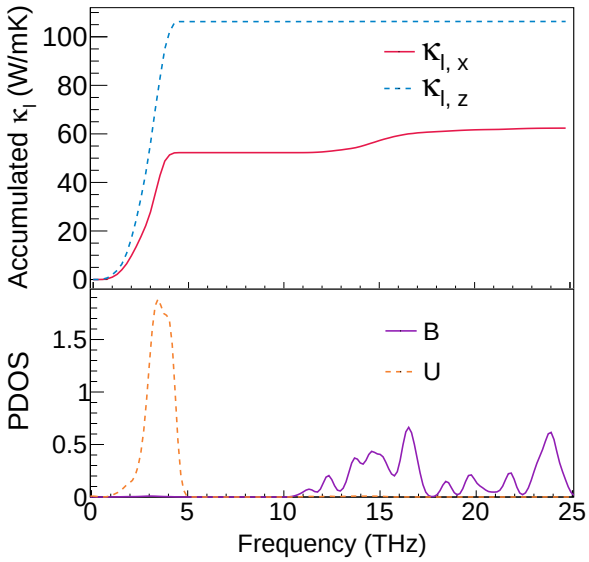

Figure 5: The calculated (a) accumulated lattice thermal conductivity at 300 K in the x and z directions, (b) the phonon density of states for UB_2 produced with Phono3py, which only takes phonon-phonon scattering into account.

Other phonon properties are related to κ_l via [53]:

$$\kappa_l = \frac{1}{3}\cdot C_v \cdot v^2 \cdot \tau_p \quad (7)$$

where C_v is the volumetric heat capacity at constant volume and τ_p is the relaxation time of the phonons. The calculated heat capacity is compared with previous experimental data in Figure 6. Phono3py [37] was used to calculate C_v from phonon-phonon interactions, whilst Phonopy [56] was used to calculate phonon properties and volumetric heat capacity at constant pressure, C_p, under the quasi harmonic approximation [57]. This was achieved through density functional perturbation theory (DFPT) calculations at a number of different volumes centered around the relaxed volume. In both calculated heat capacities the electronic contribution, γT (where $\gamma = 9.40\,\mathrm{mJ\ /\ K^2\cdot\ mol}$ [58]) is included. It can be seen that the calculation reproduces the experimental result well, particularly at low temperatures, and therefore the large discrepancy between the calculated and experimental κ_l [55] is likely due to either v or τ.

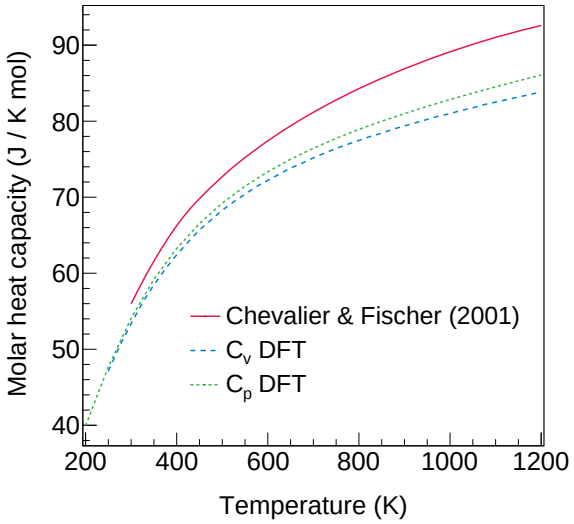

Figure 6: The experimental heat capacity of UB_2 at constant pressure [59] compared with the calculated results.

The discrepancy between the results obtained through DFT and Phono3py calculations and the available experimental data [55] could be due to an overestimated calculated phonon relaxation time. The scattering rate, which is the inverse of the phonon relaxation time, is a sum of individual scattering rates due to interactions between phonons and other phonons, defects/impurities, surfaces, magnetic entropy and electrons [23, 53] i.e.

$$\frac{1}{\tau_p} = \frac{1}{\tau_{ph-ph}} + \frac{1}{\tau_{ph-def}} + \frac{1}{\tau_{ph-sur}} + \frac{1}{\tau_{ph-spin}} + \frac{1}{\tau_{ph-e}} \quad (8)$$

Phono3py only calculates the phonon-phonon scattering effects and, optionally, the phonon-isotope scattering effect included in the phonon-defect contribution. Other defects and impurities can be included in the cell structure of DFT calculations but this removes symmetry and are therefore better suited for molecular dynamics calculations due to computational limits. The phonon-surface scattering depends on both the sample size and grain size of a physical sample, which is not included in the DFT calculations.

Table 1: Comparison of mechanical properties of UB_2 calculated in this work, with previous DFT calculations (*) and experimental measurements (†). The mechanical properties listed are the elastic constants, C_{ij}, bulk modulus, B, shear modulus, G, Young's modulus, E, Poisson's ratio, μ, sound velocity, v, and Debye temperature, θ_D.

	Elastic constants (GPa)										
Study	C_{11}	C_{12}	C_{13}	C_{33}	C_{44}	B (GPa)	G (GPa)	E (GPa)	μ	v (m/s)	θ_D (K)
This work	437	56	98	503	262	208	215	479	0.116	4500	598
*Jossou (2017) [35]	342	161	280	503	105	275	88	238	0.36	2961	392
†Dancausse (1992) [13]						225					
†Flotow (1969) [54]											394(17)

The Callaway model [60], which assumes a Debye phonon spectrum, defines lattice thermal conductivity as [23]

$$\kappa_l = \frac{k_B}{2\pi v}\left(\frac{k_B T}{\hbar}\right)^3 \int_0^{\theta_D/T} \frac{\tau_p x^4 e^x}{(e^x-1)^2} dx \tag{9}$$

where T is the temperature, $x = \hbar\omega/k_B T$ and ω is the phonon frequency. A number of the previously discussed phonon scattering rates can be fit to data with

$$\frac{1}{\tau_{ph-ph}} = UT^3 x^2 e^{-\theta_D/bT} \tag{10}$$

$$\frac{1}{\tau_{ph-sur}} = B \tag{11}$$

where U, b, and B are free parameters. As there are periodic boundary conditions and no defects or impurities present, B was first set to 0 and the Callaway model was fit to κ_l produced from DFT calculations. Following the fit, U and b were found to be $11419\,\mathrm{K}^{-3}\mathrm{s}^{-1}$ and 4.39 respectively. The parameter B responsible for phonon-boundary scattering was estimated from v and assumes a typical grain size of $7.5\,\mu$m [55], which produces a value of $6.0\times10^8\,\mathrm{s}^{-1}$. The addition of the phonon-boundary term has an insignificant impact on the total lattice thermal conductivity values.

The electron-phonon scattering rates, which are related to the imaginary part of the phonon self-energy, Π''_{qv}, within the Migdal approximation [61], are also introduced into Equations (8) and (9). When using EPW, Π''_{qv} corresponds to the phonon half-width at half-maximum, γ_{qv} [39] thus

$$\frac{1}{\tau_{ph-e}} = \frac{2\Pi''_{qv}}{\hbar} = \frac{2\gamma_{qv}}{\hbar} \tag{12}$$

where the subscripts q and v correspond to the wavevector and mode, respectively.

Three curves of κ_l are displayed in Figure 7, highlighting how the thermal conductivity changes after the introduction of each additional scattering rate. It can be seen, shown by the dotted blue line, that the interaction between phonons and electrons reduces the total lattice thermal conductivity by an order of magnitude. As κ_l is dominated by electron-phonon scattering, the effect from phonon-isotope scattering is comparatively insignificant, and therefore κ_l is effectively independent of the boron isotope ratio (unlike ZrB_2).

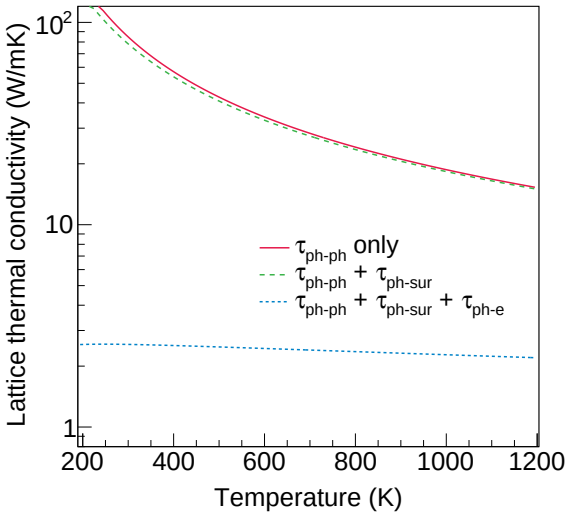

Figure 7: The lattice thermal conductivity of UB_2 according to the Callaway model, expanding the single crystal DFT calculations (τ_{ph-ph} only) with phonon-surface and phonon-electron interactions.

3.2.1. *Electronic thermal conductivity*

The resistivity of UB_2, ρ, is calculated with EPW which solves the Boltzmann transport equations, utilizing Ziman's resistivity formula [39] as an approximation solution i.e.

$$\rho(T) = \frac{4\pi m_e}{n_e e^2 k_B T}\int_0^\infty \hbar\omega\,\alpha^2_{tr}F(\omega)\,\eta(\omega,T)[1+\eta(\omega,T)]\,d\omega \tag{13}$$

where m_e is the mass of the electron, n_e is the number of electrons per unit volume, $\alpha^2_{tr}F(\omega)$ are Eliashberg transport functions and $\eta(\omega,T)$ is the Bose-Einstein distribution. At room temperature a resistivity value of $9.16\,\mu\Omega$·cm was calculated, which is comparable to the experimental measurement of a single crystal, which is approximately $10\,\mu\Omega$·cm [33].

The calculated band structure, shown in Figure 8, is similar to that of Jossou et al. [35] highlighting the validity of these results.

The total electronic contribution to the thermal conductivity, κ_e, is calculated from the impurity and phonon contributions via Matthiessen's rule [62]

$$\frac{1}{\kappa_e} = \frac{1}{\kappa_e^{imp}} + \frac{1}{\kappa_e^{ph}} \tag{14}$$

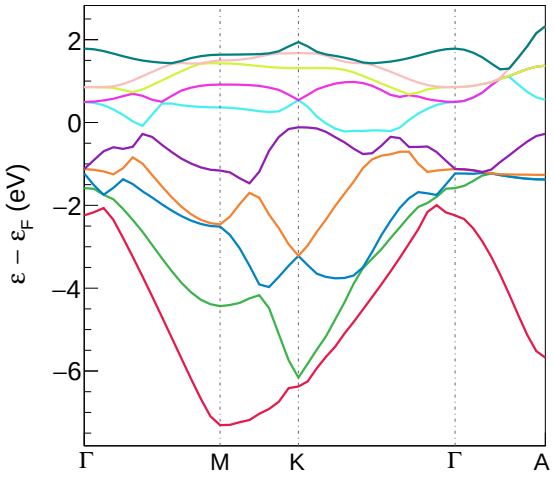

Figure 8: The calculated band structure of UB_2 exhibits metallic properties. The energy in the y-axis is reduced by the Fermi energy.

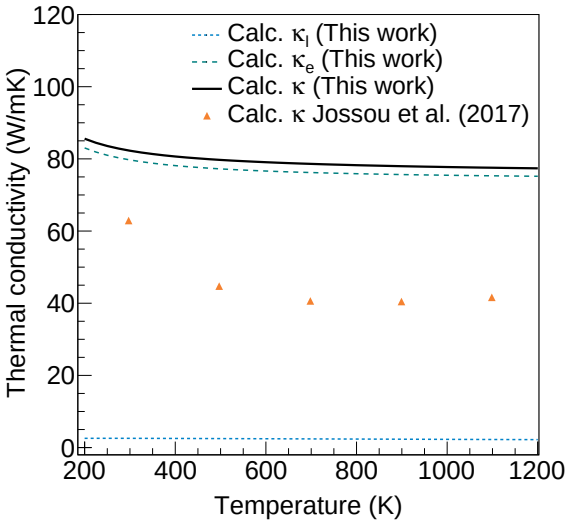

Figure 9: The total calculated thermal conductivity of UB_2, with a natural isotopic abundance of B, showing the individual lattice and electronic contributions. Previous calculations of the total lattice thermal conductivity by Jossou et al. [35]. are also shown for comparison.

where $\kappa_e^{imp} = LT/\rho$ from the Weidemann-Franz law and $L = 2.44 \times 10^{-8}$ $W\Omega K^{-2}$ [62]. The electron-phonon component is calculated via [63]

$$\frac{1}{\kappa_e^{ph}} = \frac{6\Omega}{\pi\hbar k_B N(\varepsilon) < v_e^2(\varepsilon) >} \left[\int_0^\infty \frac{d\omega}{\omega} \alpha_{tr}^2 F(\omega) \left(\frac{x}{\sinh x}\right)^2 \left(1 + \frac{x^2}{\pi^2}\right) + \int_0^\infty \frac{d\omega}{\omega} \alpha^2 F(\omega) \left(\frac{x}{\sinh x}\right)^2 \left(\frac{3x^2}{\pi^2}\right) \right] \quad (15)$$

where $x = \hbar\omega/2k_BT$, $\alpha^2F(\omega)$ are the Eliashberg transport functions and $N(\varepsilon)$ and $v_e(\varepsilon$ are the density of states per spin and the velocity at the Fermi level, ε. However, it was found that the phonons had little effect on the electronic thermal conductivity i.e. κ_e^{ph} is an insignificant contribution to κ_e.

The total thermal conductivity for UB_2 is shown in Figure 9, and compared with previous DFT calculations [35] . It can be seen that κ_e is dominant over the small κ_l values at all temperatures. There is a discrepancy between the results obtained in this work and of previous DFT calculations [35]) due to a number of factors. The κ_l values calculated by Jossou et al [35] are similar when only the phonon-phonon scattering is taken into account, as the authors did not include phonon-electron scattering. The κ_e values obtained by Jossou et al [35] were based on an approximation of ρ, based on the experimental result of UN. Therefore the discrepancy arises as ρ was calculated in this work, and compared with experimental data of UB_2. There is also a discrepancy when compared to previous experimental work [55] where the author suggests potential cracking and impurities. It is unknown what effect impurities would have on the electronic band structure of UB_2, and therefore of κ.

4. Conclusions

Through the use of DFT calculations, the phonon and electron interactions and subsequently the thermal conductivities of ZrB_2 and UB_2 have been calculated. ZrB_2 and UB_2 are similar in that they both exhibit the same hexagonal structure with layers in the basal plane. In ZrB_2 the calculation lies within the range of previous experimental data, yet the experimental κ of UB_2 is significantly lower than the calculated result [55]. The effect of impurities and surface interactions on the thermal conductivity cannot be determined easily through DFT calculations, as symmetry is removed and the calculation cost is greatly increased. It may be possible to investigate this effect through molecular dynamic calculations. The electron-phonon scattering rates calculated for UB_2 were found to be significant which reduces κ_l, and leads κ_e to be the dominant contributor to κ. An additional discrepancy was observed between κ_e calculated in this work and in previous DFT calculations [35], though it is shown that the previous work was based on experimental data from UN and not UB_2 which is addressed here.

We show that κ_l for ZrB_2 can be significantly increased when a pure isotope of B is used, but isotopic purity is a negligible contribution in UB_2 due to the large electron-phonon scattering. It is possible that variability of boron isotope enrichment could be partly responsible for the significant spread in experimental data for κ of ZrB_2, though isotope enrichment alone is not enough to explain the entire spread. An experimental study of the isotope ratio on thermal conductivity in all related diborides is encouraged for comparison.

5. Acknowledgements

This work was carried out as part of the Sêr Cymru II programme funded through the Welsh European Funding Office

(WEFO) under the European Development Fund (ERDF). Computing resources were made available by HPC Wales and Supercomputing Wales and special thanks are due to Aaron Owen, Benjamin Nash and Adrian Fewings.

References

[1] J. L. Snelgrove, G. L. Hofman, C. L. Trybus, T. C. Wiencek, Development of very-high-density fuels by the RERTR program, Tech. Rep. ANL–TD-CP-91562, Argonne National Lab. (1996).

[2] J. T. White, A. T. Nelson, J. T. Dunwoody, D. D. Byler, D. J. Safarik, K. J. McClellan, Thermophysical properties of U_3Si_2 to 1773 K, J. Nucl. Mater. 464 (2015) 275–280. doi:10.1016/j.jnucmat.2015.04.031.

[3] S. B. Ross, M. S. El-Genk, R. B. Matthews, Thermal conductivity correlation for uranium nitride fuel between 10 and 1923 K, J. Nucl. Mater. 151 (3) (1988) 318–326. doi:10.1016/0022-3115(88)90026-8.

[4] J. T. White, A. T. Nelson, Thermal conductivity of UO_{2+x} and U_4O_{9-y}, J. Nucl. Mater. 443 (1) (2013) 342–350. doi:10.1016/j.jnucmat.2013.07.063.

[5] E. Sooby Wood, J. T. White, C. J. Grote, A. T. Nelson, U_3Si_2 behavior in H_2O: Part I, flowing steam and the effect of hydrogen, J. Nucl. Mater. 501 (2018) 404 – 412. doi:10.1016/j.jnucmat.2018.01.002.

[6] S. C. Middleburgh, A. Claisse, D. A. Andersson, R. W. Grimes, P. Olsson, S. Mašková, Solution of hydrogen in accident tolerant fuel candidate material: U_3Si_2, J. Nucl. Mater. 501 (2018) 234–237. doi:10.1016/j.jnucmat.2018.01.018.

[7] D. A. Lopes, S. Uygur, K. Johnson, Degradation of UN and UN–U_3Si_2 pellets in steam environment, J. Nucl. Sci. Technol. 54 (4) (2017) 405–413. doi:10.1080/00223131.2016.1274689.

[8] W. E. Lee, M. Gilbert, S. T. Murphy, R. W. Grimes, Opportunities for Advanced Ceramics and Composites in the Nuclear Sector, J. Am. Ceram. Soc. 96 (7) (2013) 2005–2030. doi:10.1111/jace.12406.

[9] M. B. Chadwick, M. Herman, P. Obložinský, M. E. Dunn, Y. Danon, A. C. Kahler, D. L. Smith, B. Pritychenko, G. Arbanas, R. Arcilla, R. Brewer, D. A. Brown, R. Capote, A. D. Carlson, Y. S. Cho, H. Derrien, K. Guber, G. M. Hale, S. Hoblit, S. Holloway, T. D. Johnson, T. Kawano, B. C. Kiedrowski, H. Kim, S. Kunieda, N. M. Larson, L. Leal, J. P. Lestone, R. C. Little, E. A. McCutchan, R. E. MacFarlane, M. MacInnes, C. M. Mattoon, R. D. McKnight, S. F. Mughabghab, G. P. A. Nobre, G. Palmiotti, A. Palumbo, M. T. Pigni, V. G. Pronyaev, R. O. Sayer, A. A. Sonzogni, N. C. Summers, P. Talou, I. J. Thompson, A. Trkov, R. L. Vogt, S. C. van der Marck, A. Wallner, M. C. White, D. Wiarda, P. G. Young, ENDF/B-VII.1 Nuclear Data for Science and Technology: Cross Sections, Covariances, Fission Product Yields and Decay Data, Nucl. Data Sheets 112 (12) (2011) 2887 – 2996. doi:https://doi.org/10.1016/j.nds.2011.11.002.

[10] S. C. Middleburgh, L. Hallstadius, M. Puide, A sintered nuclear fuel pellet, a fuel rod, a fuel assembly, and a method of manufacturing a sintered nuclear fuel pellet, EU Patent WO2018153572 (A1).

[11] T. J. Abram, J. D. Turner, A high density composite fuel with integrated burnable absorber: U_3Si_2 – UB_2, Submitted to J. Nucl. Mater.

[12] S. C. Middleburgh, L. Hallstadius, A ceramic nuclear fuel pellet, a fuel rod, and a fuel assembly, EU Patent WO2018197105 (A1).

[13] J. P. Dancausse, E. Gering, S. Heathman, U. Benedict, L. Gerward, S. Staun Olsen, F. Hulliger, Compression study of uranium borides UB_2, UB_4 and UB_{12} by synchrotron X-ray diffraction, J. Alloy. Compd. 189 (2) (1992) 205–208. doi:10.1016/0925-8388(92)90708-H.

[14] R. L. Simmons, N. D. Jones, F. D. Popa, D. E. Mueller, J. E. Pritchett, Integral Fuel Burnable Absorbers with ZrB_2 in Pressurized Water Reactors, Nucl. Technol. 80 (3) (1988) 343–348. doi:10.13182/NT88-A34058.

[15] P. A. Burr, E. Kardoulaki, R. Holmes, S. C. Middleburgh, Defect evolution in burnable absorber candidate material: Uranium diboride, UB_2, J. Nucl. Mater. 513 (2019) 45–55. doi:10.1016/j.jnucmat.2018.10.039.

[16] S. C. Middleburgh, D. C. Parfitt, P. R. Blair, R. W. Grimes, Atomic Scale Modeling of Point Defects in Zirconium Diboride, J. Am. Ceram. Soc. 94 (7) (2011) 2225–2229. doi:10.1111/j.1551-2916.2010.04360.x.

[17] M. J. Qin, M. W. D. Cooper, E. Y. Kuo, M. J. D. Rushton, R. W. Grimes, G. R. Lumpkin, S. C. Middleburgh, Thermal conductivity and energetic recoils in UO_2 using a many-body potential model, J. Phys. Condens. Mat. 26 (49). doi:10.1088/0953-8984/26/49/495401.

[18] M. W. D. Cooper, S. C. Middleburgh, R. W. Grimes, Vacancy mediated cation migration in uranium dioxide: The influence of cluster configuration, Solid State Ionics 266 (2014) 68–72. doi:10.1016/j.ssi.2014.08.010.

[19] S. C. Middleburgh, R. W. Grimes, K. H. Desai, P. R. Blair, L. Hallstadius, K. Backman, P. Van Uffelen, Swelling due to fission products and additives dissolved within the uranium dioxide lattice, J. Nucl. Mater. 427 (1) (2012) 359–363. doi:10.1016/j.jnucmat.2012.03.037.

[20] M. W. D. Cooper, C. R. Stanek, J. A. Turnbull, B. P. Uberuaga, D. A. Andersson, Simulation of radiation driven fission gas diffusion in UO_2, ThO_2 and PuO_2, J. Nucl. Mater. 481 (2016) 125–133. doi:10.1016/j.jnucmat.2016.09.013.

[21] P. V. Nerikar, X.-Y. Liu, B. P. Uberuaga, C. R. Stanek, S. R. Phillpot, S. B. Sinnott, Thermodynamics of fission products in $UO_{2\pm x}$, J. Phys. Condens. Mat. 21 (43). doi:10.1088/0953-8984/21/43/435602.

[22] E. Torres, T. P. Kaloni, Thermal conductivity and diffusion mechanisms of noble gases in uranium dioxide: A DFT+U study, J. of Nucl. Mater. 521 (2019) 137–145. doi:10.1016/j.jnucmat.2019.04.040.

[23] K. Gofryk, S. Du, C. R. Stanek, J. C. Lashley, X.-Y. Liu, R. K. Schulze, J. L. Smith, D. J. Safarik, D. D. Byler, K. J. McClellan, B. P. Uberuaga, B. L. Scott, D. A. Andersson, Anisotropic thermal conductivity in uranium dioxide, Nat. Commun. 5. doi:10.1038/ncomms5551.

[24] G. Kresse, J. Hafner, Ab initio molecular dynamics for liquid metals, Phys. Rev. B 47 (1993) 558–561. doi:10.1103/PhysRevB.47.558.

[25] G. Kresse, J. Hafner, Ab initio molecular-dynamics simulation of the liquid-metal–amorphous-semiconductor transition in germanium, Phys. Rev. B 49 (1994) 14251–14269. doi:10.1103/PhysRevB.49.14251.

[26] G. Kresse, J. Furthmüller, Efficiency of ab-initio total energy calculations for metals and semiconductors using a plane-wave basis set, Comp. Mater. Sci. 6 (1) (1996) 15 – 50. doi:https://doi.org/10.1016/0927-0256(96)00008-0.

[27] G. Kresse, J. Furthmüller, Efficient iterative schemes for ab initio total-energy calculations using a plane-wave basis set, Phys. Rev. B 54 (1996) 11169–11186. doi:10.1103/PhysRevB.54.11169.

[28] P. E. Blöchl, Projector augmented-wave method, Phys. Rev. B 50 (1994) 17953–17979. doi:10.1103/PhysRevB.50.17953.

[29] G. Kresse, D. Joubert, From ultrasoft pseudopotentials to the projector augmented-wave method, Phys. Rev. B 59 (1999) 1758–1775. doi:10.1103/PhysRevB.59.1758.

[30] J. P. Perdew, K. Burke, M. Ernzerhof, Generalized Gradient Approximation Made Simple, Phys. Rev. Lett. 77 (1996) 3865–3868. doi:10.1103/PhysRevLett.77.3865.

[31] J. P. Perdew, K. Burke, M. Ernzerhof, Generalized Gradient Approximation Made Simple [Phys. Rev. Lett. 77, 3865 (1996)], Phys. Rev. Lett. 78 (1997) 1396–1396. doi:10.1103/PhysRevLett.78.1396.

[32] M. Methfessel, A. T. Paxton, High-precision sampling for Brillouin-zone integration in metals, Phys. Rev. B 40 (1989) 3616–3621. doi:10.1103/PhysRevB.40.3616.

[33] E. Yamamoto, Y. Haga, T. Honma, Y. Inada, D. Aoki, M. Hedo, Y. Yoshida, H. Yamagami, Y. Ōnuki, De Haas-van Alphen Effect and Energy Band Structure in UB_2, J. Phys. Soc. Jpn 67 (9) (1998) 3171–3175. doi:10.1143/JPSJ.67.3171.

[34] S. L. Dudarev, D. Nguyen Manh, A. P. Sutton, Effect of Mott-Hubbard correlations on the electronic structure and structural stability of uranium dioxide, Philos. Mag. B 75 (5) (1997) 613–628. doi:10.1080/13642819708202343.

[35] E. Jossou, L. Malakkal, B. Szpunar, D. Oladimeji, J. A. Szpunar, A first principles study of the electronic structure, elastic and thermal properties of UB_2, J. Nucl. Mater. 490 (2017) 41 – 48. doi:https://doi.org/10.1016/j.jnucmat.2017.04.006.

[36] T. Ohkochi, S.-i. Fujimori, H. Yamagami, T. Okane, Y. Saitoh, A. Fujimori, Y. Haga, E. Yamamoto, Y. Ōnuki, Observation of 5f electrons in the itinerant limit: Three-dimensional electronic structure of UB_2, Phys. Rev. B 78 (16) (2008) 165110. doi:10.1103/PhysRevB.78.165110.

[37] A. Togo, L. Chaput, I. Tanaka, Distributions of phonon lifetimes in Brillouin zones, Phys. Rev. B 91 (2015) 094306. doi:10.1103/PhysRevB.91.094306.

[38] S.-i. Tamura, Isotope scattering of dispersive phonons in Ge, Phys. Rev. B 27 (2) (1983) 858–866. doi:10.1103/PhysRevB.27.858.

[39] S. Poncé, E. R. Margine, C. Verdi, F. Giustino, EPW: Electron-phonon coupling, transport and superconducting properties using maximally localized Wannier functions, Comput. Phys. Commun. 209 (2016) 116–133. doi:10.1016/j.cpc.2016.07.028.

[40] P. Giannozzi, O. Andreussi, T. Brumme, O. Bunau, M. B. Nardelli, M. Calandra, R. Car, C. Cavazzoni, D. Ceresoli, M. Cococcioni, N. Colonna, I. Carnimeo, A. D. Corso, S. de Gironcoli, P. Delugas, R. A. D. Jr, A. Ferretti, A. Floris, G. Fratesi, G. Fugallo, R. Gebauer, U. Gerstmann, F. Giustino, T. Gorni, J. Jia, M. Kawamura, H.-Y. Ko, A. Kokalj, E. Kkbenli, M. Lazzeri, M. Marsili, N. Marzari, F. Mauri, N. L. Nguyen, H.-V. Nguyen, A. O. de-la Roza, L. Paulatto, S. Ponc, D. Rocca, R. Sabatini, B. Santra, M. Schlipf, A. P. Seitsonen, A. Smogunov, I. Timrov, T. Thonhauser, P. Umari, N. Vast, X. Wu, S. Baroni, Advanced capabilities for materials modelling with QUANTUM ESPRESSO, J. Phys. – Condens. Mat. 29 (46) (2017) 465901. doi:10.1088/1361-648X/aa8f79.

[41] G. J. K. Harrington, G. E. Hilmas, Thermal Conductivity of ZrB2 and HfB2, in: Ultra–High Temperature Ceramics: Materials for Extreme Environment Applications, John Wiley & Sons, Ltd, 2014, pp. 197–235. doi:10.1002/9781118700853.ch9.

[42] G. K. H. Madsen, J. Carrete, M. J. Verstraete, BoltzTraP2, a program for interpolating band structures and calculating semi-classical transport coefficients, Comput. Phys. Commun. 231 (2018) 140 – 145. doi:10.1016/j.cpc.2018.05.010.

[43] J. W. Zimmermann, G. E. Hilmas, W. G. Fahrenholtz, R. B. Dinwiddie, W. D. Porter, H. Wang, Thermophysical Properties of ZrB_2 and ZrB_2SiC Ceramics, J. Am. Ceram. Soc. 91 (5) (2008) 1405–1411. doi:10.1111/j.1551-2916.2008.02268.x.

[44] H. Kinoshita, S. Otani, S. Kamiyama, H. Amano, I. Akasaki, J. Suda, H. Matsunami, Zirconium Diboride (0001) as an Electrically Conductive Lattice–Matched Substrate for Gallium Nitride, Jpn. J. Appl. Phys. 40 (12A). doi:10.1143/JJAP.40.L1280.

[45] L. Zhang, D. A. Pejaković, J. Marschall, M. Gasch, Thermal and Electrical Transport Properties of Spark PlasmaSintered HfB_2 and ZrB_2 Ceramics, J. Am. Ceram. Soc. 94 (8) (2011) 2562–2570. doi:10.1111/j.1551-2916.2011.04411.x.

[46] L. Brewer, D. L. Sawyer, D. H. Templeton, C. H. Dauben, A Study of the Refractory Borides, J. Am. Ceram. Soc. 34 (6) (1951) 173–179. doi:10.1111/j.1151-2916.1951.tb11631.x.

[47] L. Toth, H. Nowotny, F. Benesovsky, E. Rudy, Der Dreistoff: Uran-Bor-Kohlenstoff, Monatshefte fr Chemie und verwandte Teile anderer Wissenschaften 92 (3) (1961) 794–802. doi:10.1007/BF00918640.

[48] H. Holleck, Legierungsverhalten von HfB_2 mit uran- und übergangsmetalldiboriden, J. Nucl. Mater. 21 (1) (1967) 14–20. doi:10.1016/0022-3115(67)90724-6.

[49] A. M. Mulokozi, Electron transfer and bonding in the intermetallic compounds of rare earths with the AlB_2-type or a closely related structure III: The thermochemistry and stability of diborides of p-, d- and f-block elements, J. Less–Common Met. 71 (1) (1980) 105–111. doi:10.1016/0022-5088(80)90105-8.

[50] R. Hill, The Elastic Behaviour of a Crystalline Aggregate, P. Phys. Soc. A 65 (5) (1952) 349–354. doi:10.1088/0370-1298/65/5/307.

[51] H. M. Ledbetter, Sound velocities and elastic-constant averaging for polycrystalline copper, J. Phys. D: Appl. Phys. 13 (10) (1980) 1879–1884. doi:10.1088/0022-3727/13/10/017.

[52] W. M. Haynes, D. R. Lide, T. J. Bruno, CRC Handbook of Chemistry and Physics: A Ready-Reference Book of Chemical and Physical Data., 97th Edition, CRC Press, 2017.

[53] L. Lou, Introduction to Phonons and Electrons, World Scientific Publishing Co. Pte. Ltd., 2003.

[54] H. E. Flotow, D. W. Osborne, P. A. G. O'Hare, J. L. Settle, F. C. Mrazek, W. N. Hubbard, Uranium Diboride: Preparation, Enthalpy of Formation at 298.15°K, Heat Capacity from 1° to 350°K, and Some Derived Thermodynamic Properties, J. Chem. Phys. 51 (2) (1969) 583–592. doi:10.1063/1.1672038.

[55] E. Kardoulaki, J. T. White, D. D. Byler, D. M. Frazer, A. P. Shivprasad, T. A. Saleh, B. Gong, T. Yao, J. Lian, K. J. McClellan, Thermophysical and mechanical property assessment of UB_2 and UB_4 sintered via spark plasma sintering, Submitted to J. Alloys Compd.

[56] A. Togo, I. Tanaka, First principles phonon calculations in materials science, Scr. Mater. 108 (2015) 1–5.

[57] A. Togo, L. Chaput, I. Tanaka, G. Hug, First-principles phonon calculations of thermal expansion in Ti_3SiC_2, Ti_3AlC_2, and Ti_3GeC_2, Phys. Rev. B 81 (2010) 174301. doi:10.1103/PhysRevB.81.174301.

[58] E. Yamamoto, T. Honma, Y. Haga, Y. Inada, D. Aoki, N. Suzuki, R. Settai, H. Sugawara, H. Sato, Y. Ōnuki, Electrical and Thermal Properties of UB_2, J. Phys. Soc. Jpn 68 (3) (1999) 972–975. doi:10.1143/JPSJ.68.972.

[59] P. Y. Chevalier, E. Fischer, Thermodynamic modelling of the CU and BU binary systems, J. Nucl. Mater. 288 (2) (2001) 100–129. doi:10.1016/S0022-3115(00)00713-3.

[60] J. Callaway, Model for Lattice Thermal Conductivity at Low Temperatures, Phys. Rev. 113 (4) (1959) 1046–1051. doi:10.1103/PhysRev.113.1046.

[61] B. Fu, G. Tang, Y. Li, Electronphonon scattering effect on the lattice thermal conductivity of silicon nanostructures, Phys. Chem. Chem. Phys. 19 (42) (2017) 28517–28526. doi:10.1039/C7CP04638C.

[62] U. Mizutani, Introduction to the Electron Theory of Metals, Cambridge University Press, 2003.

[63] P. B. Allen, New method for solving Boltzmann's equation for electrons in metals, Phys. Rev. B 17 (10) (1978) 3725–3734. doi:10.1103/PhysRevB.17.3725.